Catalysis Letters, Vol. 118, Nos. 1–2, October 2007 (© 2007)
DOI: 10.1007/s10562-007-9133-6

Steam reforming of ethanol on Ni–CeO_2–ZrO_2 catalysts: Effect of doping with copper, cobalt and calcium

Prakash Biswas and Deepak Kunzru*

Department of Chemical Engineering, Indian Institute of Technology, Kanpur, UP 208016, India

Received 20 April 2007; accepted 20 April 2007

Steam reforming (SR) and oxidative steam reforming (OSR) of ethanol were investigated over undoped and Cu, Co and Ca doped Ni/CeO_2–ZrO_2 catalyst in the temperature range of 400–650 °C. The nickel loading was kept fixed at 30 wt.% and the loading of Cu and Co was varied from 2 to 10 wt% whereas the Ca loading was varied from 5 to 15 wt.%. The catalysts were characterized by various techniques, such as surface area, temperature programmed reduction, X-Ray diffraction and H_2 chemisorption. For Cu and Co doped catalyst, CuO and Co_3O_4 phases were detected at high loading whereas for Ca doped catalyst, no separate phase of CaO was found. The reducibility and the metal support interactions were different for doped catalysts and varied with the amount and nature of dopants. The hydrogen uptake, nickel dispersion and nickel surface area was reduced with the metal loading and for the Co loaded catalysts the dispersion of Ni and nickel surface area was very low. For Cu and Ca doped catalysts, the activity was increased significantly and the main products were H_2, CO, CH_4 and CO_2. However, the Co doped catalysts showed poor activity and a relatively large amount of C_2H_4, C_2H_6, CH_3CHO and CH_3COCH_3 were obtained. For SR, the maximum enhancement in catalytic activity was obtained with in the order of NCu5. For Cu–Ni catalysts, CH_3CHO decomposition and reforming reaction was faster than ethanol dehydrogenation reaction. Addition of Cu and Ca enhanced the water gas shift (WGS) and acetaldehyde reforming reactions, as a result the selectivity to CO_2 and H_2 were increased and the selectivity to CH_3CHO was reduced significantly. The maximum hydrogen selectivity was obtained for Catalyst N (93.4%) at 650 °C whereas nearly the same selectivity to hydrogen (89%) was obtained for NCa10 catalyst at 550 °C. In OSR, the catalytic activity was in the order N > NCu5 > NCa15 > NCo5. In the presence of oxygen, oxidation of ethanol was appreciable together with ethanol dehydrogenation. For SR reaction, the highest hydrogen yield was obtained on the undoped catalyst at 600 °C. However, with calcium doping the hydrogen yields are higher than the undoped catalyst in the temperature range of 400–550 °C.

KEY WORDS: nickel; Ni–Cu; Ni–Ca; Ni–Co; CeO_2–ZrO_2; catalysts; steam reforming; oxidative steam reforming; ethanol; hydrogen production.

1. Introduction

Use of hydrogen as an energy carrier for mobile and stationary power applications is expected to increase in the future. Steam reforming of ethanol is a potentially attractive method of producing hydrogen because, compared to other liquid feedstocks, ethanol is non-toxic, easy to handle and can be obtained from renewable feedstocks such as biomass [1–4]. Moreover, production of hydrogen by ethanol steam reforming is CO_2 neutral [5]. Steam reforming over noble metals (Pd, Pt, Rh) and nonnoble metals (Ni, Cu, Co) has been extensively studied, and recently reviewed [6,7]. Ethanol conversion and H_2 production varies greatly with reaction conditions, type of catalyst and support, as well as the method of catalyst preparation. Nickel seems to be the preferred active metal because of its high activity and low cost.

Steam reforming of ethanol has been investigated on nickel supported on various oxides such as Al_2O_3, MgO, La_2O_3, SiO_2, Y_2O_3, CeO_2 or CeO_2–ZrO_2 [5,8]. Reforming of ethanol at low temperature (250 °C) over Ni/Y_2O_3, Ni/La_2O_3 and Ni/Al_2O_3 was investigated by Sun et al. [9]. Ni/Y_2O_3 and Ni/La_2O_3 catalyst exhibited relatively higher activity in terms of ethanol conversion and hydrogen selectivity whereas Ni/Al_2O_3 was the least active. Frusteri et al. [10, 11] studied the steam reforming of bioethanol over Ni/MgO and Ni/CeO_2. Fatsikostas and Verykios [12] investigated ethanol reforming over Ni catalysts supported on γ-Al_2O_3, La_2O_3 and La_2O_3/γ-Al_2O_3. The impregnation of Al_2O_3 with La_2O_3 reduced carbon deposition. Aupretre et al. [13] reported nickel supported on CeO_2–ZrO_2 to be a very effective catalyst for steam reforming of ethanol. They tested various supports (Al_2O_3, 12%CeO_2– Al_2O_3, CeO_2, CeO_2–ZrO_2, ZrO_2) and reported that the activity in the SR reaction varies directly as the degree of mobility of surface OH groups, and selectivity towards CO_2 was controlled by the activity in the water-gas shift (WGS) reaction. The ceria-based catalysts were highly active for the WGS. In our previous study [14], we have studied the effect of metal loading and support composition of Ni–CeO_2–ZrO_2 catalysts and found that 30 wt.%

*To whom correspondence should be addressed.
E-mail: dkunzru@iitk.ac.in

$Ni/Ce_{0.74}Zr_{0.26}O_2$ to be the most effective catalyst. The enhanced activity of CeO_2–ZrO_2 mixed oxide for oxidation reaction has been reported to be due to higher oxygen mobility and formation of a solid solution [15,16].

Dopants can significantly affect the activity, selectivity and stability of catalysts. Very limited information is available on the effect of dopants during SR of ethanol. Frusteri et al. [10,11] studied the effect of alkali (Na, K, Li) addition on the behavior of Ni/MgO catalysts. Li and Na promoted the NiO reduction but negatively affected the dispersion of the Ni/MgO catalyst, whereas K did not significantly affect either the morphology or dispersion. Li and K enhanced the stability of Ni/MgO mainly by depressing Ni sintering. Marino et al. [17–20] tested Cu–Ni–K/γ–Al_2O_3 catalyst for ethanol steam reforming reaction. Copper–nickel catalysts on γ–Al_2O_3 and doped with potassium hydroxide, were suitable for hydrogen production at a relatively low temperature of 300 °C. Cu was active agent for steam reforming, Ni favored the C–C bond rupture and potassium neutralized the acidic sites of the support. In the steam reforming of hydrocarbons, Lisboa et al. [21] reported that, addition of Ca and Mg to α-Al_2O_3 supported nickel-based catalyst improve the stability and selectivity. Ca and Mg favored the steam methane reforming reaction and in presence of Mg the coke was easily oxidized. Youn et al. [22] studied the effect of second metal (Ce, Co, Cu, Mg and Zn) addition on Ni/ γ-Al_2O_3 catalysts in the auto-thermal reforming of ethanol. Among the dopants tested, Cu was found to be most efficient promoter and it was active for WGS. In addition to that, Cu also served as a barrier to prevent the growth of Ni particles and decreased the interaction between Ni-species and γ-Al_2O_3 which facilitated the reduction of Ni–Cu/γ-Al_2O_3 catalyst. A series of CuNiZnAl multi component mixed metal oxide catalysts with various Cu/Ni ratio was tested for OSR of bio-ethanol by Velu et al. [23]. Nickel significanty reduced the carbon products. Dehydrogenation of ethanol to acetaldehyde reaction was favored over Cu based catalyst whereas introduction of Ni favored the C–C bond rupture. The effect of different dopants (Cr, Fe, Zn or Cu) on Ni/Al_2O_3 catalysts for OSR of ethanol was investigated by Fierro et al. [24]. Nickel promoted the SR and WGS reactions while Al_2O_3 promoted the dehydration reaction. Moreover, Cu was more active for methane steam reforming compared to Cr, Zn and Fe. In related studies on steam reforming of methane on nickel catalysts, it has been reported that Cu enhanced the WGS activity as well as the stability of the nickel based catalyst [25,26]. Recently, Hu and Lu [27] reported that Ni–Co bimetallic catalyst was active for acetone reforming reaction and the catalyst was stable for long time without deactivation.

The influence of oxygen on product selectivity and catalyst stability has been investigated by various authors on several catalyst systems [28–30]. They concluded that an oxidizing environment is required in order to avoid carbon poisoning and to promote decomposition C_2-compounds. For the steam reforming of ethanol on Ni/Cu, it was found that addition of small amounts of oxygen increased the over all hydrogen yields and the formation of CH_4 and CO was strongly reduced [5]. Higher oxygen concentration reduced the production of hydrogen and catalyst sintered due to formation of hot spot.

Our earlier study [14] on the effect of support and metal loading on Ni/CeO_2–ZrO_2 had shown that the best performance was obtained with 30 wt% Ni on $Ce_{0.74}Zr_{0.26}O_2$. Therefore, to study the effects of dopants, this catalyst was doped with other metals. In this study, the effect of doping Ni/CeO_2–ZrO_2 catalyst with copper, cobalt or calcium on steam reforming and oxidative steam reforming of ethanol has been investigated.

2. Experimental

2.1. Preparation of catalysts

The CeO_2–ZrO_2 mixed oxide support was prepared by co-precipitation with ammonia using aqueous solution of cerium nitrate and zirconium oxychloride. Aqueous ammonia solution was added dropwise to the aqueous solution containing the Ce and Zr salt at the appropriate composition with constant stirring until pH was 9–10. After precipitation, the obtained hydroxide was filtered, washed thoroughly with deionized water, and then dried at 120 °C for 12 h. The dried solid was calcined in air at 750 °C for 5 h. The resulting solid oxide was crushed and sieved to a size 50–80 mesh before metal impregnation. The 30 wt% Ni/$Ce_{0.74}Zr_{0.26}O_2$ (Catalyst N) was prepared by incipient wetness impregnation method. After impregnation, the catalyst was dried at 120 °C for 12 h and then calcined at 500 °C for 5 h.

Cobalt, copper or calcium was added to Catalyst N by incipient wetness impregnation using an aqueous solution of cobalt nitrate, cupric nitrate or calcium nitrate. After impregnation, the doped catalysts were dried at 120 °C for 12 h and then calcined at 500 °C for 5 h. The loading of Cu was varied from 2 to 10 wt% of the total catalyst; the corresponding catalysts have been designated as NCu2, NCu5 and NCu10, respectively. Similarly, the Co and Ca doped catalysts have been designated as NCo2, NCo5, NCo10 and NCa5, NCa10, NCa15, respectively.

2.2. Characterization of catalysts

The specific surface area of catalysts was determined by the dynamic pulsing technique on a Micromeritics Pulse Chemisorb 2705 instrument, employing nitrogen

physio-sorption at liquid nitrogen temperature. Prior to each measurement, the sample was degassed at 120 °C by passing helium for 20 min.

X-ray powder diffraction (XRD) analysis was performed in order to identify the different phases present in the catalyst and to determine their crystallinity. The spectra were obtained with a Siemmens diffractometer (Model D500) using Cu Kα radiation, Ni filter and 40 kV, at a two theta interval of 20–100° with a sweep of 3°/min and a time constant of 3 sec. The average crystallite size of CeO_2 and ZrO_2 was determined using the Scherrer equation [31] from the line widths of the XRD peaks corresponding to (111), (220) and (311) crystal planes, and the average crystal size of NiO was determined from the line width of the (111), (200) and (220) crystal planes, respectively.

Temperature programmed reduction (TPR) was performed to determine the reduction behavior of CeO_2–ZrO_2 and the Ni, Cu, Co and Ca species on the support. The experiments were performed on the Micromeritics Pulse Chemisorb 2705 equipment, using 25 mg of catalyst and a temperature ramp from 35 to 1000 °C at 10 °C/min. A flow rate of 40 cm^3/min of 5% H_2 in Ar was used for the reduction. A thermal conductivity detector (TCD) was employed to determine the amount of hydrogen consumed.

The nickel surface area was determined by hydrogen pulse chemisorption on the Micromeritics Pulse Chemisorb 2705 unit. For these measurements, approximately 100 mg of catalyst was used. The catalyst was reduced at 700 °C using pure H_2 for 3 h and then the sample was purged by passing Ar at 700 °C for 1 h. The catalyst was cooled to 50 °C in flowing Ar. The hydrogen pulse chemisorption study was done using pure H_2, the pulse was given after 3–5 min interval until the area of successive hydrogen peaks were identical. The amount of carbon deposited on the catalyst after SR and OSR reaction was determined by CHNS elemental analysis using an Elemental Analyzer (Model: CE440, Leeman Labs Inc., USA). Approximately 5 mg of used catalyst was taken and treated in the presence of oxygen at 960 °C. The CO_2 produced by the oxidation of the sample was analyzed by a thermal conductivity detector.

2.3. Catalyst testing

Experiments were performed at atmospheric pressure in a continuous fixed bed downflow vertical tubular reactor consisting of a quartz tube, 320 mm in length and 10 mm i.d. Another quartz tube of 420 mm length and 5 mm i.d attached to the first one served as the outlet to facilitate fast removal of reactor effluent. The catalyst was placed on a quartz wool bed inside the reactor. 100 mg of catalyst (size: 50–80 mesh) diluted with 150 mg of same sized quartz particles was used for catalytic tests. Prior to a run, the catalyst was reduced in situ at 650 °C for 1 h under a hydrogen flow rate of 20 cc/min. Water/ethanol mixture ($EtOH/H_2O$ = 1:8 mol/mol) premixed in a separate container, vaporized at 150 °C was fed to the reactor by a pump (Model RP-G6; FMI, USA). Nitrogen, which served as an inert, was mixed with the vaporized feed, and the mixture was then fed to the reactor. The flow rate of nitrogen was controlled by a mass flow controller. To study the effect of oxygen addition in the feed on the catalytic activity and product selectivity, the O_2/EtOH molar ratio was fixed at 0.5. The liquid flow rate was maintained at 0.08 mL/min and the reaction temperature was varied from 400 to 650 °C. The product stream was analyzed by use of three gas chromatographs (Nucon). The first one, equipped with a packed column (Hysep) and a flame ionization detector (FID) with N_2 as the carrier gas, was used for the separation of CO, CH_4, CO_2, C_2H_4, C_2H_6, C_2H_5OH, CH_3CHO and CH_3COCH_3. The second GC, equipped with a Molecular Sieve 5 A column and TCD with Ar as the carrier gas, was used for the determination of H_2. The third GC was used to analyze the composition of condensed liquid products, on a capillary column (Petrocol DH capillary column) using FID with N_2 as the carrier gas. For calculating the selectivity of the gaseous products, nitrogen was used as the internal standard. For the liquid products, iso-propanol was used as the internal standard. Reaction gases were supplied from high pressure gas cylinders and analytical grade ethanol (99.99% pure, s.d.Fine-Chem, ltd. Mumbai, India) was used for the reaction. For the reported runs, the carbon balance was 100 ± 5%.

The selectivity of carbon containing products has been defined as:

$$S_X(\%) = \frac{\text{moles of carbon in product } X}{\text{total moles of carbon in products}} \times 100$$

and the selectivity to hydrogen as:

$$S_{H_2}(\%) = \frac{\text{moles of } H_2 \text{ produced}}{\text{total moles of hydrogen in products}} \times 100$$

3. Results and discussion

3.1. Catalyst characterization

The surface area of catalysts and the crystallite size of CeO_2–ZrO_2 and NiO are shown in Table 1. The surface area of catalyst N was 19.5 m^2/g and decreased after doping with Cu, Co or Ca. For Cu doped catalyst, with an increase in Cu loading from 2 to 10 wt.%, the surface area decreased from 13.9 to 11.6 m^2/g. The surface area of Co doped catalysts was almost the same as the Cu doped catalysts. For Ca doped catalysts, the surface area was less than half the surface area of the undoped catalyst.

Table 1
Structural parameters and specific surface area of different catalyst

Catalyst	CeO_2–ZrO_2 crystallite size (nm)	NiO-crystallite size (nm)	Surface area (m^2/g)
N	12.5	17.3	19.5
NCu2	11.4	12.3	13.9
NCu5	10.2	12.5	12.4
NCu10	11.2	12.5	11.6
NCo2	10.8	11.4	11.4
NCo5	10.9	12	10.9
NCo10	10.4	11.4	10.8
NCa5	11.7	12.9	7.55
NCa10	12.2	12.1	6.62
NCa15	12.1	14.1	5.28

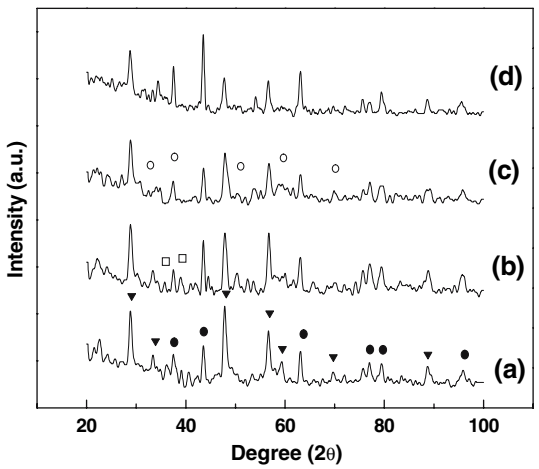

Figure 1. XRD patterns of catalysts, (a) N, (b) NCu10, (c) NCo10, (d) NCa15. (▼) CeO_2–ZrO_2, (●) NiO, (□) CuO, (○) Co_3O_4.

The XRD patterns of the catalysts N, NCu10, NCo10 and NCa15 are shown in figure 1. For Catalyst N, the presence of diffraction peaks at 2θ = 29°, 33°, 48° and 56° correspond respectively to the planes of CeO_2 (111), CeO_2 (200), ZrO_2 (220), CeO_2 (311), and the peaks at 2θ = 37°, 43° and 62° correspond respectively to the (111), (200) and (220) crystal planes of NiO. For catalyst NCu10, the additional peaks at 2θ values of 33.7° and 39° represent the presence of CuO phase [17,18]. At lower Cu loading, no peak corresponding to CuO was detected. For the Co doped catalyst, diffraction peaks at 2θ values of 32°, 37°, 45°, 59° and 65° indicate the presence of Co_3O_4 [32]. At lower Co loading, the intensity of these peaks was not significant. Therefore, the XRD patterns of Cu and Co catalysts with lower loading have not been shown. No separate phase of CaO was detected in the Ca doped catalysts. The dimensions of CeO_2–ZrO_2 and NiO crystallites in Catalyst N were 12.5 and 17.3 nm, respectively (table 1). After doping, there was a marginal decrease in the crystallite size of the support whereas the NiO crystallite size reduced by 20–30%. For doped catalysts, the crystallite size of CeO_2–ZrO_2 was in the range of 10.2–12.2 nm and NiO crystallite size was in the range of 12.1–14.1 nm, respectively (table 1).

The reduction features of the catalysts were analyzed by TPR. The TPR plots of Catalyst N and Cu doped catalyst are shown in figure 2. For sake of comparison, the TPR of 10 wt.% Cu supported on $Ce_{0.74}Zr_{0.26}O_2$ was also obtained (figure 2a). The TPR plot exhibited three overlapping reduction peak at 164°C, 229°C and 270°C respectively. Similar TPR results have been reported for the reduction of CeO_2 supported CuO catalysts [33,34]. For catalyst N, a combined broad peak was obtained (figure 2b); the first peak (320°C) corresponds to the reduction of NiO particles having a lower interaction with the support and the second peak (370°C) is associated with the reduction of NiO strongly bonded to the support. In the TPR of Cu doped catalysts (figure 2c, d and e), four reduction peaks were observed. Depending on the Cu content, the peaks were in the temperature range of 148–149 °C, 186–194 °C, 302–317 °C and 699–710 °C, respectively. The first two peaks correspond to the reduction of CuO, the third peak is associated with the combined reduction of NiO and CuO and the low intensity peak at 700 °C is due to the reduction of bulk CeO_2. From TPR plots, it can be noticed that the broadness of the peak at 302 °C increased with copper loading. The TPR plots show that with Cu addition, the nickel oxide was reduced at a lower temperature.

The TPR plots of Co doped catalysts together with the TPR plot of 10 wt% Co–$Ce_{0.74}Zr_{0.26}O_2$ are shown in figure 3. The TPR of 10% Co–$Ce_{0.74}Zr_{0.26}O_2$ (figure 3a) showed a low intensity peak at 310 °C and a broader peak at 350°C. The peak obtained at 310 4°C corresponds to the reduction of Co_3O_4 to CoO, and the peak at 350 °C has been attributed to the reduction of CoO to metallic Co [35,36]. The broad peak at 741 °C is due to the reduction of bulk CeO_2. The TPR plot of NCo2 catalyst (figure 3b) was characterized by one sharp peak

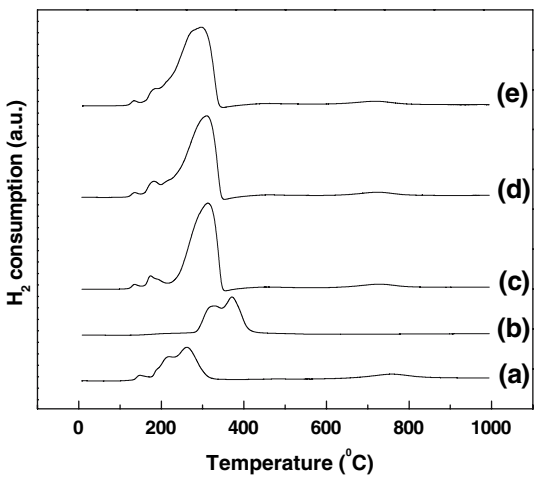

Figure 2. TPR profile of fresh catalysts. (a) 10 wt% Cu–$Ce_{0.74}Zr_{0.26}O_2$, (b) N, (c) NCu2, (d) NCu5, (e) NCu10.

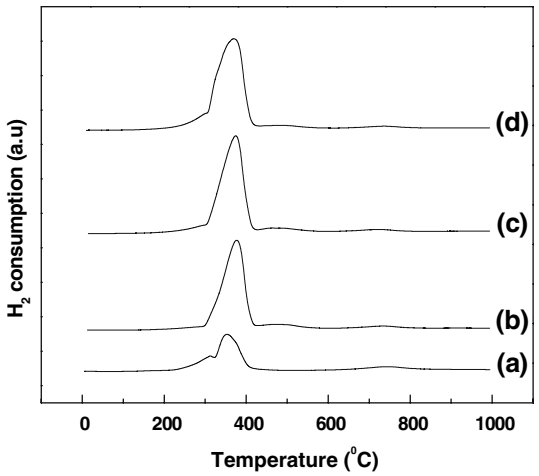

Figure 3. TPR profile of fresh Co doped catalyst, (a) 10 wt% Co–$Ce_{0.74}Zr_{0.26}O_2$, (b) NCo2, (c) NCo5, (d) NCo10.

at 379 °C which corresponds to the combined reduction of NiO, Co_3O_4 and CoO. With an increase in Co loading, this peak shifted towards lower temperature indicating that the higher loaded catalysts were more reducible.

The TPR profiles of Ca doped nickel catalyst as well as 10 wt% Ca on $Ce_{0.74}Zr_{0.26}O_2$ are shown in figure 4. The TPR profile of 15 wt% Ca–$Ce_{0.74}Zr_{0.26}O_2$ catalyst (figure 4a) was characterized by two peaks; one at 600 °C for the reduction of CaO and another low intensity peak at 737 °C corresponding to the reduction of bulk CeO_2. For NCa5 catalyst, three reduction peaks were obtained (figure 4b); a combined peak at a temperature of 317 °C corresponding to the reduction of loosely and strongly bounded NiO to Ni°, the second one at a temperature of 472 °C corresponding to the reduction of CaO and a peak at 699 °C corresponding to the reduction of bulk CeO_2. With an increase in Ca

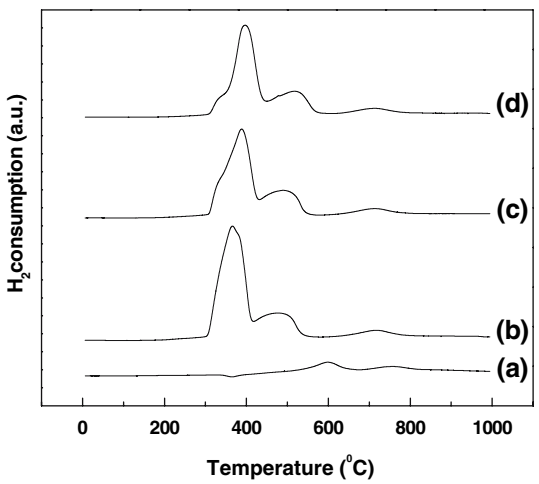

Figure 4. TPR profile of fresh Ca doped catalyst, (a) 10 wt% Ca–$Ce_{0.74}Zr_{0.26}O_2$, (b) NCa5, (c) NCa10, (d) NCa15.

loading, nature of the nickel oxide reduction peak changed. At a loading of 10 and 15 wt.% Ca, a shoulder at around 325 °C can be seen, indicating that the proportion of loosely bonded NiO reduced with Ca loading. Moreover, the reduction temperature of the strongly bonded NiO increased with Ca loading, i.e., with increasing Ca loading, the metal-support interaction increased.

The hydrogen uptake, nickel dispersion and nickel surface area of the catalysts obtained from hydrogen pulse chemisorption are shown in the table 2. For calculation of dispersion, it was assumed that the stoichiometry of chemisorption of hydrogen atom on nickel was 1 and hydrogen did not chemisorb on Cu, Co or Ca. As can be seen from table 2, the H_2 uptake, nickel dispersion and Ni surface area decreased with increasing metal loading. The calculated nickel dispersion and nickel surface areas waere in the range of 0.02–0.30% and 0.01–0.30 m^2/g, respectively. The dispersion of Ni and the nickel surface area in the Co loaded catalyst was very low.

3.2. Catalytic performance in steam reforming

The effect of temperature on catalytic activity and selectivity of the catalysts was examined at the same space velocity (W/F_{A0} = 4.06 gcat.h.mol^{-1}). Ethanol conversion as a function of time on stream was measured for 15 h. Initially, the activity declined rapidly but after 4 h, the rate of deactivation was very slow. Therefore, all the reported data were collected after a run time of 4 h. For Catalyst N, the effect of temperature on ethanol conversion and product selectivities is shown in figure 5. Conversion increased with temperature and was >90% at 500 °C. The main products were H_2, CO, CH_4, and CO_2 but at a lower temperature (<450 °C) significant amount of CH_3CHO was also obtained. Selectivity to CH_3CHO decreased exponentially with temperature. With increasing temperature, selectivity to CO_2 and H_2 increased, selectivity to CH_4 decreased whereas the CO selectivity passed through a minima at 500 °C. The maximum hydrogen selectivity

Table 2
H_2 pulse chemisorptions results of different catalysts

Catalyst	H_2-uptake (μ mol/g cat)	Dispersion (%)	Ni surface area (m^2/g cat)
N	7.60	0.30	0.30
NCu2	7.11	0.28	0.28
NCu5	5.47	0.23	0.21
NCu10	4.24	0.18	0.16
NCo2	2.02	0.09	0.08
NCo5	1.41	0.06	0.02
NCo10	0.55	0.02	0.01
NCa5	6.46	0.27	0.25
NCa10	5.44	0.24	0.21
NCa15	4.23	0.2	0.16

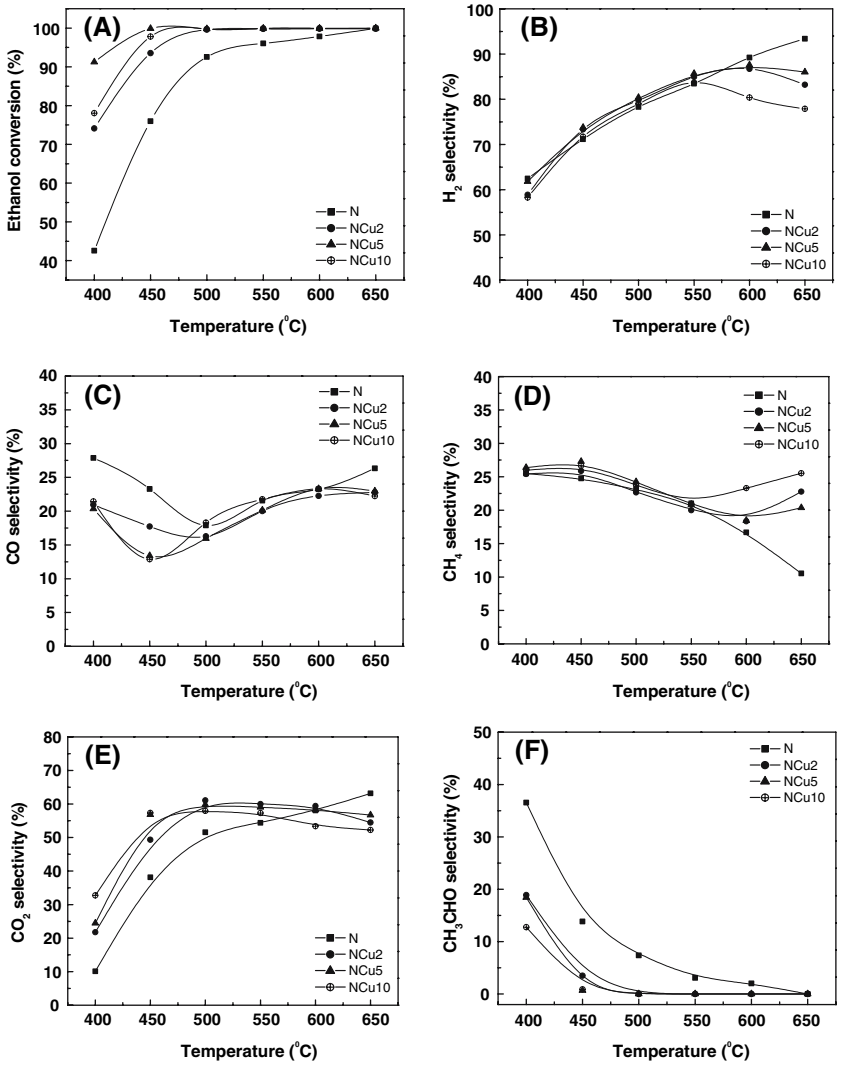

Figure 5. Variation of ethanol conversion and product selectivities with temperature. Effect of Cu doping. (A) Conversion; (B) H_2 selectivity; (C) CO selectivity; (D) CH_4 selectivity; (E) CO_2 selectivity; (F) CH_3CHO selectivity.

of 93.4% was obtained at a temperature of 650 °C. At this temperature, the ethanol conversion was 100% and the selectivities to CO, CH_4 and CO_2 were 26.3%, 10.5% and 63.2% respectively.

In our earlier study [14], the product distribution obtained over undoped Ni/CeO_2–ZrO_2 catalysts could be explained by the following reaction scheme:

$$C_2H_5OH \rightarrow CH_3CHO + H_2 \quad (1)$$

$$C_2H_5OH \rightarrow C_2H_4 + H_2O \quad (2)$$

$$CH_3CHO \rightarrow CH_4 + CO \quad (3)$$

$$CH_3CHO + H_2O \rightarrow 2CO + 3H_2 \quad (4)$$

$$CH_4 + H_2O \rightarrow CO + 3H_2 \quad (5)$$

$$CO + H_2O \rightarrow CO_2 + H_2 \quad (6)$$

$$2CH_3CHO \rightarrow CH_3COCH_3 + CO + H_2 \quad (7)$$

For undoped catalysts, at high temperatures, the product composition is mainly controlled by methane reforming reaction and the water–gas shift reaction.

3.2.1. *Effect of Cu*

The catalytic behavior of Cu doped catalysts is also shown in figure 5. As shown in figure 5A, the activity of catalysts increased significantly with Cu doping. The effect of Cu doping on conversion was more at lower temperatures (< 500 °C). At 400 °C, the ethanol conversion increased from 43 to 74% by addition of 2 wt.%Cu (NCu2) and conversion was 91% at 400 °C for catalyst NCu5. Further increase in copper loading

had an adverse effect on the conversion and for NCu10, conversion decreased to 78% at 400 °C. For all Cu doped catalysts, the conversion was 100% at a temperature of 500 °C and higher.

The variation of product selectivities for Cu doped catalyst at different temperatures is shown in figure 5. For all Cu doped catalysts, selectivity to H_2 showed a maxima with increasing temperature (figure 5B) and was highest for NCu5. Selectivity to CO showed a minima with increasing temperature (figure 5C). The effect of Cu doping on CO selectivity was appreciable below at 450 °C. At temperatures of 500 °C and above, the CO selectivity for NCu2 and NCu5 catalyst was similar. The minimum CO selectivity (≈13%) was obtained at 450 °C for Catalysts NCu5 and NCu10. For Cu doped catalysts, selectivity to CH_4 showed a minima with increasing temperature (figure 5D). For catalysts NCu2 and NCu5, the minimum CH_4 selectivity was obtained at 600 °C, whereas for NCu10 the minima was observed at 550 °C. Selectivity to CH_4 for undoped and Cu doped catalysts was not significantly different till 550 °C. Selectivity to CO_2 for Cu doped catalysts increased sharply in the temperature range of 400–500 °C, but did not change significantly above 500 °C (figure 5E). Below 500 °C, CO_2 selectivity increased with Cu doping. Selectivity to CH_3CHO decreased with an increase in temperature and copper content of the catalyst. For all the doped catalyst, the selectivity was zero at temperature of 500 °C and higher.

It is well-known that an effective catalyst for ethanol reforming should be capable of breaking the C–C bond and also be active for water gas shift (WGS). Earlier studies have shown that Ni favors the C–C bond rupture but its activity for the WGS is low [13,37,38]. On the other hand, Cu is known to be a good catalyst for WGS and the active sites for reforming and WGS are the reduced metallic species [22]. For steam reforming of methane, Huang and Jhao [39] reported that copper increases the WGS activity and thereby the overall steam reforming reaction activity is enhanced. The TPR data shows that with an increase in Cu loading, the reduction temperature of Ni species was lower, implying that the interaction between the support and nickel decreased. For steam reforming of CH_4 over Ni and Ni–Cu catalysts, addition of Cu into a Ni catalyst enhanced the WGS activity and the enhancement was related to the amount of bimetallic Cu–Ni species [40]. In our study, the activity increased with copper content till a loading of 5 wt.%, but decreased at higher loading. This is most likely due to the formation of a segregated CuO phase as evidenced by XRD. A similar effect of Cu loading of Ni–Cu/γ-Al_2O_3 catalysts was reported for autothermal reforming of ethanol where a 5 wt.% Cu containing catalyst was more active than either a 2 wt.% or 7 wt.% Cu containing Ni–Cu catalyst [22].

The product distribution shows that for undoped catalyst at lower temperature (400 °C), significant amount of acetaldehyde was formed due to dehydrogenation of ethanol (reaction 1). However, for Cu–Ni catalysts, CH_3CHO formation reduced significantly implying that in the presence of Cu, CH_3CHO decomposition and reforming (reaction 3 and 4 respectively) are faster than ethanol dehydrogenation. With addition of Cu, selectivity to CO reduced significantly with a simultaneous increase in the selectivities to H_2 and CO_2. This confirms that Cu enhanced the WGS activity as has also been reported by others [14,22]. At 450 °C, acetaldehyde decomposition was complete, and the effluent gas composition was then controlled by the two reversible reactions of methane steam reforming (MSR), reaction 5 and WGS, reaction 6. The observed trend of the product selectivity changes can be explained on the basis of these two reactions. Below 450 °C, the rate of WGS is not significant and consequently the selectivity to CO_2 is low. As the temperature increased to 450 °C, the rates of WGS and MSR become significant resulting in a lower selectivity to CO and CH_4 together with a higher selectivity to H_2 and CO_2. Klouz et al. [29] also reported a decrease in the selectivity to CO in the temperature range of 300–400 °C during the ethanol reforming on Ni–Cu/SiO_2.

The selectivity trends for Cu–Ni catalysts show that at high temperature the reverse WGS and reverse MSR reactions, start to control the product distribution. As a result, the selectivities to CO and CH_4 increase whereas the selectivities to H_2 and CO_2 decrease. This is in contrast to the undoped catalyst where the selectivity to CH_4 decreased with temperature suggesting that the reverse methane reforming reaction was not appreciable. Previous studies [41,42] have also reported that, for Cu based catalyst at higher temperature, the reverse WGS reaction is significant. Suetsuna et al. [43] reported, that for Cu–Ni based catalyst at higher temperature, more methane was produced leading to the simultaneous consumption of CO and H_2 according to the reverse MSR.

3.2.2. *Effect of Ca*

The ethanol conversion and product selectivities for Ca doped catalysts are shown in figure 6. Activity of the catalysts increased significantly with addition of Ca to the catalyst. As shown in figure 6A, conversion of ethanol increased with the amount of Ca incorporated in the catalysts. For all Ca doped catalysts, conversion was nearly 100% at a temperature of 550 °C and above. The main products were H_2, CO, CH_4 and CO_2. These are the products of both steam reforming and water gas shift reactions that take place simultaneously in the reactor. Minor amount of CH_3CHO was observed at lower temperature. The product selectivities were also affected due to Ca doping, especially at lower temperatures (< 500 °C). In the temperature range of 400–550 °C, selectivity to H_2 and CO_2 (figure 6B&E) was higher for Ca doped catalysts whereas the

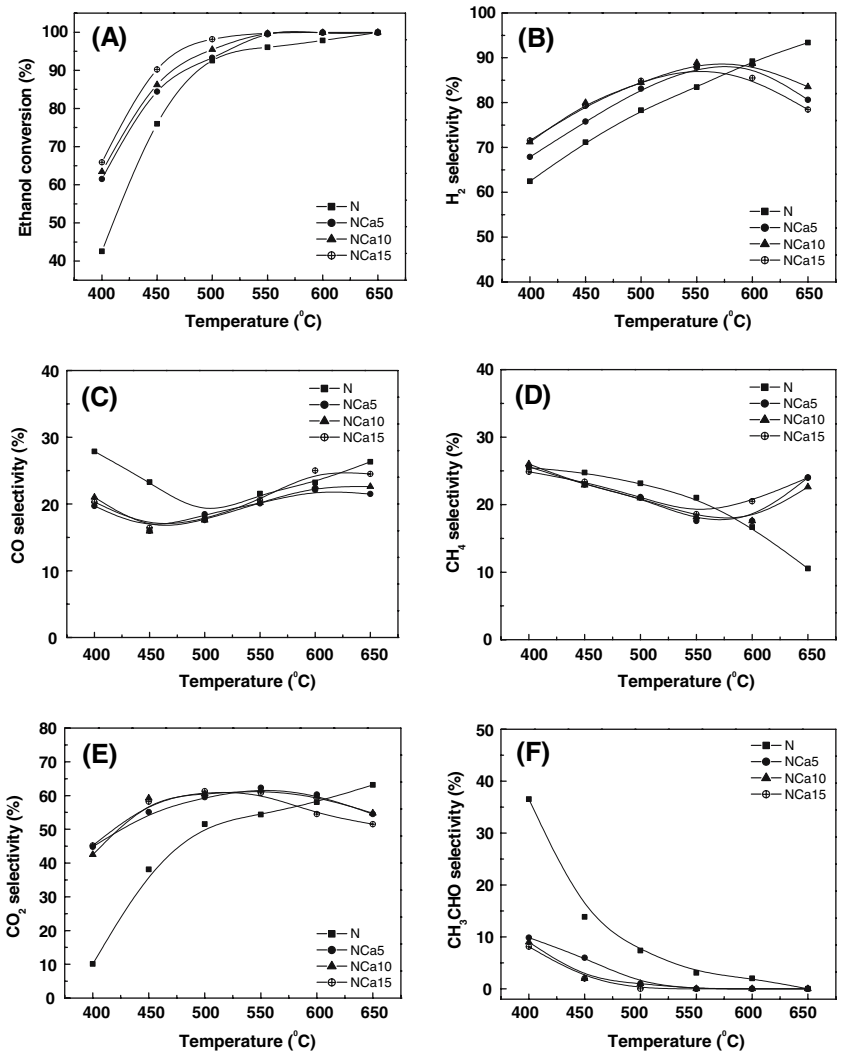

Figure 6. Variation of ethanol conversion and product selectivities with temperature. Effect of Ca doping (A) Conversion; (B) H_2 selectivity; (C) CO selectivity; (D) CH_4 selectivity; (E) CO_2 selectivity; (F) CH_3CHO selectivity.

selectivities to CO and CH_3CHO were lower (figure 6C&F). Selectivity to CH_4 (figure 6D) was not affected significantly till 550 °C; at higher temperature the selectivity of CH_4 increased slightly.

The data shows that in the presence of Ca, ethanol dehydrogenation reaction was inhibited and the WGS reaction was enhanced, thereby increasing the overall activity for the SR. No previous studies on the effect of calcium doping on the catalyst activity during ethanol reforming have been reported but Zhang and Baerns [44] in their study of oxidative methane coupling have reported that CaO–CeO_2 catalyses the WGS. Also, Xu et al. [45], in their study of gasification of Ca-impregnated coffee grounds, reported that Ca catalyses the WGS. In contrast to Cu–Ni/CeO_2–ZrO_2 catalysts, for Ca–Ni catalysts, the activity does not correlate with the ease of reduction of the catalyst. Even though the reduction temperature of the nickel oxide marginally increased with calcium loading, the activity also increased. A possible reason for the enhancement in activity could be the effect of Ca on the electronic properties of the Ni clusters. Chang et al. [46] reported the beneficial effect of calcium doping on Ni/ZrO_2 catalysts for dry reforming of methane. They reported that alkaline-earth promoters can affect the physico chemical properties of nickel reforming catalysts by affecting the electronic properties of the Ni catalysts, or by increasing the basic character of the support. For SR of ethanol on Ni/MgO catalysts, Freni et al. [47] reported that MgO inhibited the dehydrogenation of ethanol and also contributed to the electronic enhancement of Ni. The variation of product selectivities with temperature was similar to that obtained with Ca doped catalysts. The main difference was that at lower (400 °C), the selectivity to CO_2 and H_2 were higher and the selectivity to CH_3CHO was lower than that obtained for Cu doped catalysts. This implies that acetaldehyde reforming and WGS were faster than on Ca doped catalysts. At a temperature of 550 °C and above, the reverse WGS and MSR reaction controlled the product selectivity as a

result, the selectivity to H_2 and CO_2 decreased and CO and CH_4 selectivity increased.

3.2.3. Effect of Co

The conversion and product distribution obtained with Co doped catalysts is shown in table 3. Conversion of ethanol for these catalysts was significantly lower than the undoped catalysts, especially at lower temperatures (<500 °C). Above 500 °C, the main products were H_2, CO, CH_4 and CO_2, but at lower temperature (<450 °C) the selectivity of these products was very low whereas the selectivity to CH_3CHO and CH_3COCH_3 was relatively higher. Measurable amounts of C_2H_4 and C_2H_6 were obtained at all temperatures. With an increase in temperature, selectivity to CO_2 increased and the selectivity to H_2 passed through a maxima.

At lower temperature (400 °C), the product selectivity trend of Co doped catalyst signifies that the steam reforming reaction did not proceed appreciably over these catalysts and mainly ethanol dehydrogenation (reaction 1), decarbonylation of acetaldehyde (reaction 7) and WGS reaction (reaction 6) were favored. The relatively large amount of CH_3COCH_3 and relatively low concentration of CH_4 at lower temperature indicates that Co has weaker capability of breaking the C–C bond in ethanol molecule. Previous studies have reported Co on different supports (Al_2O_3, ZnO, SiO_2, V_2O_5 etc.) to be less active for ethanol SR and more active for ethanol dehydrogenation to acetaldehyde, ethanol dehydrogenation to ethylene and ethanol decomposition to acetone [35,47,48]. Batista et al. [32] observed that the oxidized cobalt species was not active for SR of ethanol whereas Co metal was the active agent for the catalytic process. Llorca et al. [49] studied the SR of bioethanol on ZnO-supported cobalt catalysts and concluded that Co_3O_4 and CoO did not have a positive effect on the SR reaction. The product distribution obtained in this study may be due to the cobalt species, their amount and states on the surface of the catalyst and also their interaction with the support and Ni metal present in the catalyst. The XRD showed that Co_3O_4 was present on cobalt doped Ni/CeO_2–ZrO_2, which can also convert to CoO under the reaction conditions. The presence of these two oxides may result in the reduced activity. Another reason for the lower activity could be the very low nickel surface area of these catalysts (refer table 2). At higher temperature (>550 °C), the activity increased and significant amount of H_2, CO, CH_4 and CO_2 was obtained but still side products were also present.

3.3. Catalytic performance in oxidative steam reforming

The effect of oxygen addition on steam reforming was investigated for Catalyst N, NCu5, NCo15 and NCa15. For these runs, the total volumetric flowrate was kept the same as for the earlier steam reforming runs. For the reported data, H_2O/EtOH and O_2/EtOH molar ratios were 8:1 and 0.5:1, respectively. The reaction temperature was varied from 400–650 °C. The variation of conversion and product distributions with temperature for OSR for the four catalysts is shown in figure 7. During oxidative steam reforming, the catalyst activity varied as in the order: N > NCu5 > NCa15 > NCo5. For all the catalysts, conversion increased due to oxygen addition. Except for NCo5, conversion for the other catalyst was 100% at a temperature of 450 °C and higher. The undoped catalyst showed the highest activity in OSR. In all cases, with an increase in temperature,

Table 3
Catalytic behavior of Co doped catalyst-N in the steam reforming of ethanol

Catalyst	Temperature (°C)	Ethanol conversion (%)	% Selectivity of products							
			CO	CH_4	CO_2	C_2H_4	C_2H_6	CH_3CHO	CH_3COCH_3	H_2
NCo2	400	25.7	0.4	0.4	14.8	2.1	1.4	39.3	36.6	35.5
	450	40.6	0.9	0.70	20.5	3.4	1.2	36.5	36.1	54.0
	500	74.2	22.4	18.2	35.3	8.5	1.1	14.5	0.00	73.7
	550	86.6	20.9	21.1	36.5	9.5	0.8	9.3	1.8	75.8
	600	99.6	23.5	23.5	51.3	0.9	0.9	0.0	0.00	81.1
	650	99.6	24.5	23.1	51.2	0.7	0.4	0.0	0.00	80.7
NCo5	400	29.5	0.6	0.7	15.0	1.7	1.5	46.8	33.3	37.5
	450	39.6	0.6	0.6	20.9	4.3	1.1	24.0	47.0	54.7
	500	66.5	21.3	21.6	35.9	1.7	0.8	14.3	3.9	69.9
	550	78.7	23.8	21.8	39.2	2.9	0.9	9.9	1.3	75.8
	600	96.2	22.8	22.3	42.9	5.9	1.1	4.8	0.0	75.5
	650	99.6	24.0	23.7	41.5	8.1	1.8	0.8	0.0	74.1
NCo10	400	33	0.4	0.4	17.5	3.3	1.3	38.8	37.8	32.2
	450	47.6	26.4	23.9	18.0	1.5	0.7	18.4	10.9	55.8
	500	71.7	24.6	21.8	37.6	1.8	0.8	12.0	1.2	69.5
	550	82	20.9	17.0	43.5	5.8	1.0	11.6	0.0	75.3
	600	98.4	24.1	22.3	48.1	0.9	1.8	2.7	0.0	72.7
	650	99.8	21.9	23.9	48.8	3.4	2.0	0.0	0.0	69.6

selectivities to H_2 and CO_2 passed through a maxima, selectivity to CO showed a minima and selectivity to CH_3CHO decreased. Except for NCo5, selectivity to CH_4 showed a decreasing trend with temperature and the selectivity to CH_3CHO was zero above 450 °C for the other catalysts.

In comparison to steam reforming, during OSR over NCa15 the selectivity to CH_4 was lower at a temperature of 550 °C and above whereas H_2, CO selectivities were lower in the whole temperature range. The selectivity to CO_2 was higher at higher temperature. For NCu5, selectivity to H_2 reduced but other product selectivities were not significantly affected due to the addition of oxygen. For NCo5, selectivities to CO and CH_4 increased significantly at lower temperature but at higher temperature (> 500 °C), these selectivities were not significantly affected compared to the selectivities obtained in the absence of oxygen. Selectivity to H_2 and CO_2 increased significantly with temperature. During SR reaction over NCo5 catalyst, considerable amounts of side products such as ethylene, ethane, acetaldehyde and acetone were obtained but in OSR reaction the side products reduced drastically.

3.3.1. *Effect of oxygen*

The products selectivity profile suggest that the OSR reaction does not occur in single reaction step between ethanol, water and oxygen but the actual process is the combination of several overlapping exothermic and endothermic reactions steps. Velu et al. [23] made thermodynamic equilibrium composition calculations for SR and OSR at atmospheric pressure. They found that the calculated equilibrium compositions for SR and OSR were not too different. Their calculations also showed that addition of oxygen decreased the CH_4 selectivity with a simultaneous increase in the selectivity of CO_2. However, for their study of ethanol reforming on $Cu_{1-x}Ni_xZnAl$-mixed metal oxide catalysts, the product distribution showed that the reactions were not at equilibrium. Cavallaro et al. [50] studied the steam reforming of ethanol on Rh/Al_2O_3 catalyst and reported only small changes in CO_2 CO and CH_4 selectivity due to addition of 0.4 vol.% of oxygen to the feed. In presence of O_2, the following additional reaction can take place:

$$H_2 + 1/2O_2 = H_2O \quad (8)$$

$$CO + 1/2O_2 = CO_2 \quad (9)$$

$$CH_4 + 1/2O_2 = CO_2 + 2H_2O \quad (10)$$

$$2CH_3CHO + 5O_2 = 4CO_2 + 4H_2O \quad (11)$$

$$C_2H_5OH + 3O_2 = 2CO_2 + H_2O \quad (12)$$

The maximum increase in catalytic activity and change of product selectivity was observed over NCo5 catalyst below 500 °C. The increase in selectivity of CO, CH_4, CO_2, H_2 and the significant decrease in a selectivity of C_2–C_3 compounds is most likely due to enhanced oxidation of the side products.

In presence of O_2, different catalysts showed different product selectivities but the trend for most of the products was similar (figure 7). In all cases, the catalyst activity was higher and selectivity to CH_3CHO significantly lower which suggests that in addition to ethanol dehydrogenation, oxidation of ethanol was also appreciable. Moreover CH_3CHO can also reacted with oxygen to form carbon oxides [51]. Oxygen favored the CO oxidation reaction as a result a large amount of CO_2 was obtained in OSR process compared to SR, especially at higher temperature. The data suggests that WGS reaction plays an important role in determining the product selectivities. With an increase in temperature from 400 to 500 °C, the CO, CH_4 and CH_3CHO selectivities decreased with a concomitant increase in H_2 selectivity. This implies that in this temperature range, the WGS reaction was not at equilibrium. The increase in CO selectivity at high temperature is due to contribution of the reverse WGS. Other reactions which affect the product distribution are methane reforming, oxidation of H_2 and CH_4. The lower hydrogen selectivity in the presence of oxygen is due to the oxidation of hydrogen (reaction 8). The decreasing trend of CH_4 selectivity was obtained due to the combustion of methane in presence of oxygen.

The effect of oxygen on hydrogen yields at different temperatures for the undoped and doped catalysts is shown in table 4. For SR reaction, the highest hydrogen yield was obtained on the undoped catalyst at 600 °C. However, with calcium doping the hydrogen yields are higher than the undoped catalyst in the temperature range of 400–550 °C. For OSR, the hydrogen yield with Ca-doped catalyst at 550 °C was nearly equal to the yield obtained for undoped catalyst at 650 °C. Thus, with calcium doping the reaction temperature can be significantly reduced without affecting the hydrogen yields.

3.4. *TPR of used catalysts*

The TPR studies were carried out for the used catalysts both after steam reforming (SR) as well as oxidative steam reforming (OSR). The results are shown in figure 8. By comparing the TPR results of used and fresh undoped catalyst (Catalyst N), the peaks obtained at 238 °C and 256 °C can be attributed to the reduction of NiO to Ni° and the peaks obtained at 513 °C and 494 °C (figure 8A(a) & B(a)) for the reduction of CeO_2. Therefore, from the results, it can be observed that the NiO was not completely reduced after reforming and CeO_2 was present in the used catalyst. No significant reduction peaks were observed during the TPR of used Cu and Co doped catalysts. For both the catalysts, a very low

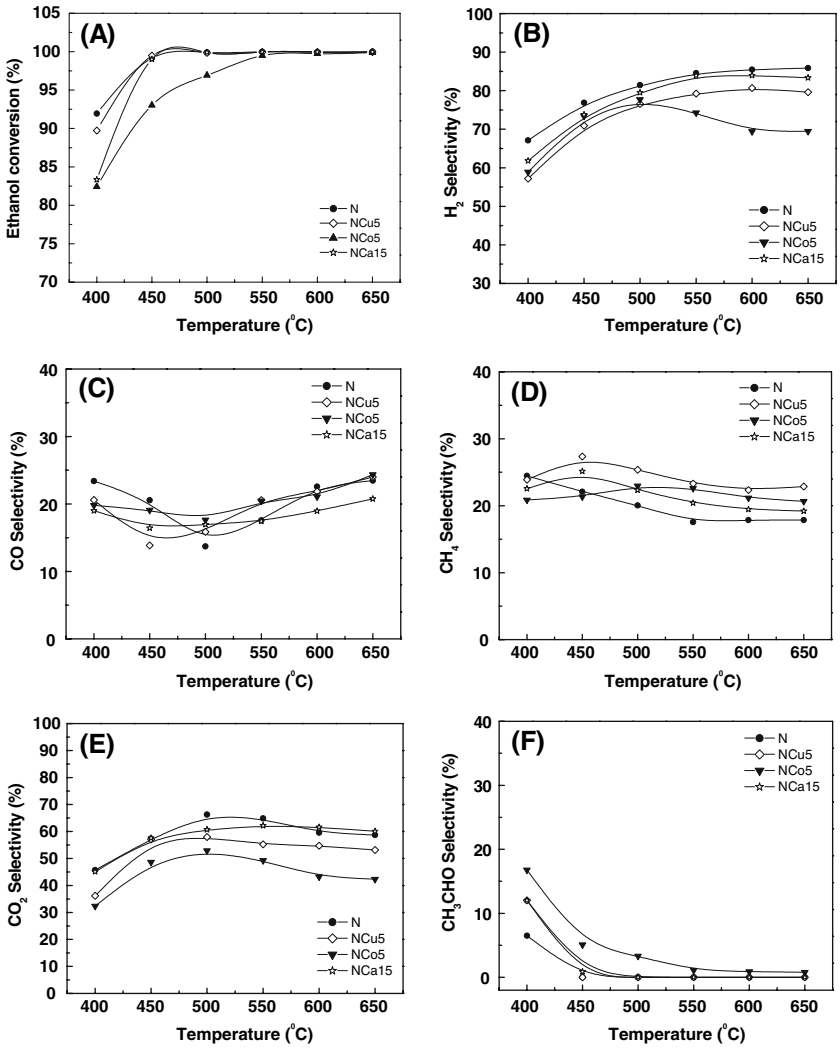

Figure 7. Variation of ethanol conversion and product selectivities with temperature in OSR. Effects of Cu, Co, and Ca doping (A) Conversion; (B) H_2 selectivity; (C) CO selectivity; (D) CH_4 selectivity; (E) CO_2 selectivity; (F) CH_3CHO selectivity.

intensity peak was obtained in the temperature range of 267–414 °C, which may be due to reduction of small amount of NiO present in the used catalyst. This suggests that the catalysts were almost completely reduced after steam reforming (SR) as well as oxidative steam reforming (OSR). However, for Ca doped catalyst, for SR and OSR reaction, one broad peak was obtained at a temperature of 544 °C and 575 °C, respectively and another peak was obtained at 673 °C and 693 °C, respectively (figure 8A(d) & B(d)). A comparison of the TPR profiles of the used and fresh Ca doped catalysts (figure 4d), shows that the used catalyst was not reduced completely. The TPR profile of the used catalyst was similar to that of the fresh catalyst; only the reduction temperature was shifted towards higher temperature.

3.5. Coke formation

The amount of carbon deposited on the catalysts after 15 h of run time was measured by CHNS elemental analysis. As shown in figure 9, for all the doped and undoped catalysts, considerable amounts of carbon were formed in SR and OSR. In SR, the coke formation rate is comparable for catalyst N and NCo5 whereas the coke formation rate is highest for NCu5 and lowest for NCa15. It is known that, in the reforming of ethanol, carbon formation takes place by the dissociation of hydrocarbon molecule formed during reaction or the dissociation of CO according to Bouduard reaction [52]. The carbon formation strongly depends on the reaction conditions as well as the surface properties of the catalysts. The high carbon formation for NCu5, NCo5 and N, may be due to the low nickel area of the catalyst or a low metal support interaction [53,54]. The nickel particles present on the surface of the catalyst may favor the Bouduard reaction and ethanol decomposition which promotes the carbon formation. In presence of Ca, the carbon formation is less, presumably due to the increase in the electronic properties of nickel clusters by calcium which reduces the Bouduard reaction and hydrocarbon

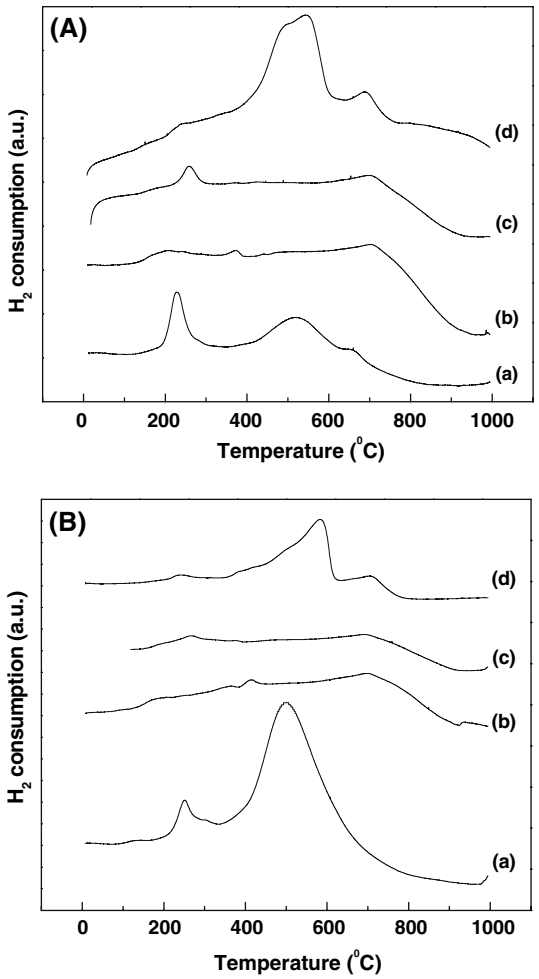

Figure 8. TPR profile of used catalyst (A) After SR of ethanol (a) N, (b) NCu5 (c) NCo5, (d) NCa15. (B) After OSR of ethanol (a) N, (b) NCu5 (c) NCo5, (d) NCa15.

decomposition activity of the catalyst [46,55]. In the steam reforming of bio-ethanol, coke formation was reduced significantly by the addition of alkali (Li, Na, K) on Ni/MgO catalysts [56]. For all the catalysts, in presence of oxygen rate of coke formation was reduced significantly. The maximum decrease in rate of coke formation was observed for NCu5.

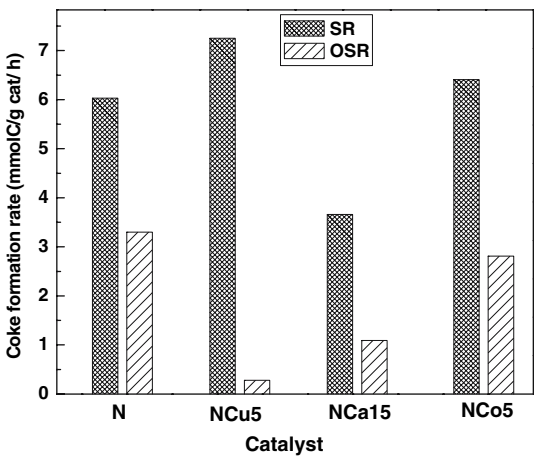

Figure 9. Coke formation rate in SR and OSR at 600 °C; W/F_{A0} = 4.06 gcat h mol^{-1}; O_2/EtOH = 0.5 (for OSR).

Table 4
Variation of hydrogen yield with temperature in SR and OSR of ethanol

Catalyst	Temperature (°C)	Hydrogen yield, mol of H_2/mol of ethanol fed	
		SR of ethanol	OSR of ethanol
N	400	0.89	2.08
	450	2.2	2.92
	500	3.26	3.52
	550	4.23	3.57
	600	5.66	4.23
	650	5.63	4.34
NCu5	400	2.43	1.67
	450	3.2	2.76
	500	3.96	3.38
	550	4.99	3.7
	600	5.21	3.87
	650	5.01	3.57
NCo5	400	0.3	1.62
	450	0.77	2.78
	500	2.03	3.66
	550	2.91	3.13
	600	3.39	2.7
	650	3.36	2.53
NCa15	400	1.85	1.58
	450	3.38	2.85
	500	4.63	3.51
	550	5.33	4.33
	600	4.84	4.07
	650	3.49	3.85

4. Conclusions

Addition of copper, calcium or cobalt affects the physicochemical properties of the Ni/CeO_2–ZrO_2 catalyst as well as the activity and product selectivities during steam reforming of ethanol. The extent of interaction varied with the nature and amount of dopants. At low loadings of Cu and Co and for all other loadings of Ca, no new phases were detected by XRD confirming the formation of mixed solid solution. At high loading of Cu and Co, segregated CuO and Co_3O_4 phases were detected. The TPR results showed that catalysts doped with Cu or Co were more reducible whereas calcium enhanced the metal-support interaction and the reduction temperature of strongly bonded NiO increased with Ca loading. The hydrogen uptake, nickel dispersion and nickel surface area reduced with metal loading and for the Co loaded catalysts the dispersion of Ni and nickel surface area was very low. Copper and Ca addition enhanced the reforming and WGS activity of the catalysts and simultaneously reduced the ethanol

dehydrogenation. The Co doped catalysts was less active and a relatively large amount of C_2H_4, C_2H_6, CH_3CHO and CH_3COCH_3 were obtained. Among the second metals tested, Ca was the most efficient dopant for the production of hydrogen; the WGS activity was higher for Ca doped catalysts than Ni–Cu catalysts. In comparison to the hydrogen selectivity obtained with Catalyst N in SR process, nearly the same amount (5.75 mol/mol ethanol reacted) of hydrogen was obtained for NCa10 catalyst at a lower temperature (550 °C). In OSR process, the catalytic activity decreased in the order N > NCu5 > NCa15 > NCo5. In all the cases, the catalyst activity was higher and selectivity to CH_3CHO was significantly lower due to oxidation of ethanol and ethanol dehydrogenation. Over NCo5 catalyst, below 500 °C, the maximum increase in catalytic activity and the selectivity to CO, CH_4, CO_2, and H_2 was observed due to enhanced oxidation of the side products. The selectivity of C_2–C_3 compounds was also reduced significantly. For SR reaction, the highest hydrogen yield was obtained on the undoped catalyst at 600 °C. However, with calcium doping the hydrogen yields are higher than the undoped catalyst in the temperature range of 400–550 °C. For OSR, the hydrogen yield with Ca-doped catalyst at 550 °C was nearly equal to the yield obtained for undoped catalyst at 650 °C. Therefore, Ca may be a good promoter of ceria–zirconia supported nickel catalysts for SR and OSR of ethanol for production of ethanol.

References

[1] F. Marino, M. Boveri, G. Baronetti and M. Laborde, Int. J. Hydrogen Energy 26 (2001) 665.
[2] J.P. Breen, R. Burch and H.M. Coleman, Appl. Catal. B: Environ. 39 (2002) 65.
[3] D.K. Liguras, D.I. Kondarides and X.E. Verykios, Appl.Catal. B: Environ. 43 (2003) 345.
[4] M.A. Goula, S.K. Kontou and P.E. Tasiakaras, Appl. Catal. B: Environ. 49 (2004) 135.
[5] A.N. Fatsikostas, D.I. Kondarides and X.E. Verykios, Catal. Today 75 (2002) 145.
[6] P.D. Vaidya and A.E. Rodrigues, Chem. Eng. J. 117 (2006) 39.
[7] A. Haryanto, S. Fernando, N. Murali and S. Adhikari, Energy Fuels 19 (2005) 2098.
[8] Y. Yang, J. Ma and F. Wu, Int. J. Hydrogen Energy 31(7) (2006) 877.
[9] J. Sun, X.P. Qiu, F. Wu and W.T. Zhu, Int. J. Hydrogen Energy 30 (2005) 437.
[10] F. Frusteri, S. Freni, V. Chiodo, L. Spadaro, O. Di Blasi, G. Bonura and S. Cavallaro, Appl. Catal. A: Gen. 270 (2004) 1.
[11] F. Frusteri, S. Freni, V. Chiodo, S. Donato, G. Bonura and S. Cavallaro, Int. J Hydrogen Energy 31 (2006) 2193.
[12] A.N. Fatsikostas and X.E. Verykios, J. Catal. 225 (2004) 439.
[13] F. Aupretre, C. Descorme and D. Duprez, Catal. Commun. 3 (2002) 263.
[14] P. Biswas and D. Kunzru, Int. J. Hydrogen Energy (2006), doi: 10.1016/j.ijhydene.2006.09.031.
[15] T.X.T. Sayle, S.C. Parker and C.R.A. Catlow, Surf. Sci. 316 (2004) 329.
[16] C. Leitenburg, A. Trovarelli, J. Llorca, F. Cavani and G. Bini, Appl. Catal. A: Gen. 139 (1996) 161.
[17] F.J. Marino, E.G. Cerrella, S. Duhalde, M. Jobbagy and M.A. Laborde, Int. J. Hydrogen Energy 23(12) (1998) 1095.
[18] F. Marino, M. Boveri, G. Baronetti and M. Laborde, Int. J. Hydrogen Energy 26 (2001) 665.
[19] F. Marino, G. Baronetti, M. Jobbagy and M. Laborde, Appl. Catal. A: Gen. 238 (2003) 41.
[20] F. Marino, M. Boveri, G. Baronetti and M. Laborde, Int. J. Hydrogen Energy 29 (2004) 67.
[21] J.S. Lisboa, D.C.R.M. Santos, F.B. Passos and F.B. Noronha, Catal. Today 101 (2005) 15.
[22] M.H. Youn, J.G. Seo, P. Kim, J.J. Kim, H.I. Lee and I.K. Song, J. Power Sources 162(2) (2006) 1270.
[23] S. Velu, K. Suzuki, M. Vijayaraj, S. Barman and C.S. Gopinath, Appl. Catal. B: Environ 55 (2005) 287.
[24] V. Fierro, O. Akdim, H. Provendier and C. Mirodatos, J. Power Sources 145 (2005) 659.
[25] J.H. Lee, E.G. Lee, O.S. Joo and K.D. Jung, Appl. Catal. A: Gen 269 (2004) 1.
[26] T.J. Huang, T.C. Yu and S.Y. Jhao, Ind. Eng. Chem. Res. 45 (2006) 150.
[27] X. Hu and G. Lu, J. Mol. Catal. A: Chem. 261 (2007) 43.
[28] S. Cavallaro, V. Chiodo, A. Vita and S. Freni, J. Power Sources 123 (2003) 10.
[29] V. Klouz, V. Fierro, P. Denton, H. Katz, J.P. Lisse, S. Bouvot-Mauduit and C. Mirodatos, J. Power sources 105 (2002) 26.
[30] E. Vesselli, G. Comelli, R. Rosei, S. Freni, F. Frusteri and S. Cavallaro, Appl. Catal. A: Gen 281 (2005) 139.
[31] A.M. Arias, M.F. Garcia, V. Ballesteros, L.N. Salamanca, J.C. Conesa, C. Otero and J. Soria, Langmuir 15 (1999) 4796.
[32] M.S. Batista, R.K.S. Santos, E.M. Assaf, J.M. Assaf and E.A. Ticianelli, J. Power Sources 124 (2003) 99.
[33] P. Araya, S. Guerrero, J. Robertson and F.J. Gracia, Appl. Catal. a: Gen. 283 (2005) 217.
[34] J. Papavasiliou, G. Avgouropoulos and T. Ioannides, Appl. Catal B: Environ. 69 (2007) 226.
[35] B. Zhang, X. Tang, Y. Li, W. Cai, Y. Xu and W. Shen, Catal. Commun. 7 (2006) 367.
[36] M.S. Batista, E.M. Assaf, J.M. Assaf and E.A. Ticianelli, Int. J. Hydrogen Energy 31 (2006) 1204.
[37] J.H. Sinfelt and D.J.C. Yates, J. Catal. 8 (1967) 82.
[38] J. Comas, F. Marino, M. Laborde and N. Amadeo, Chem. Eng. J. 98 (2004) 61.
[39] T.J. Huang and S.Y. Jhao, Appl. Catal. A: Gen. 302 (2006) 325.
[40] T.J. Huang, T.C. Yu and S.Y. Jhao, Ind. Eng. Chem. Res. 45 (2006) 150.
[41] S. Patel and K.K. Pant, J. Power Sources 159 (2006) 139.
[42] C.Z. Yao, L.C. Wang, Y.M. Liu, G.S. Wu, Y. Cao, W.L. Dai, H.Y. He and K.N. Fan, Appl. Catal. A: Gen. 297 (2006) 151.
[43] T. Suetsuna, S. Suenaga and T. Fukasawa, Appl. Catal. A: Gen. 276 (2004) 275.
[44] Z. Zhang and M. Baerns, Appl. Catal. 75 (1991) 299.
[45] G. Xu, T. Murakami, T. Suda, Y. Matsuzawa, H. Tani, Y. Mito and M. Ashizawa, AIChE 52(10) (2006) 3555.
[46] J.S. Chang, D.Y. Hong, X. Li and S.E. Park, Catal. Today 115 (2006) 186.
[47] S. Freni, S. Cavallaro, N. Mondello, L. Spadaro and F. Frusteri, Catal. Commun. 4 (2003) 259.
[48] J. Llorca, N. Homs, J. Sales and P.R. Piscina, J. Catal. 209 (2002) 306.
[49] J. Llorca, P.R. Piscina, J.A. Dalmon, J. Sales and N. Homs, Appl. Catal. B: Environ. 43 (2003) 355.

[50] S. Cavallaro, V. Chiodo, S. Freni, N. Mondello and F. Frusteri, Appl. Catal. A: Gen 249 (2003) 119.
[51] E.M. Cordi, P.J. O'Neill and J.L. Falconer, Appl. Catal. B: Environ. 14(1–2) (1997) 23.
[52] N. Laosiripojana and S. Assabumrungrat, Appl. Catal. B: Environ. 66 (2006) 29.
[53] Y.H. Hu and E. Ruckenstein, Catal. Lett. 42 (1996) 145.
[54] N. Nichio, M. Casella, O. Ferretti, M. González, C. Nicot, B. Moraweck and R. Frety, Catal. Lett. 42 (1996) 65.
[55] J.A.C. Dias and J.M. Assaf, Catal. Today 85 (2003) 59.
[56] F. Frusteri, S. Freni, V. Chiodo, L. Spadaro, O. Di Blasi, G. Bonura and S. Cavallaro, Appl. Catal. A: Gen. 270 (2004) 1.